SCIENCE CHINA
Information Sciences

• RESEARCH PAPER •

January 2022, Vol. 65 112303:1–112303:16
https://doi.org/10.1007/s11432-020-3164-5

CS-LTP-Spinal: a cross-layer optimized rate-adaptive image transmission system for deep-space exploration

Shaohua WU*, Dongqing LI, Jian JIAO & Qinyu ZHANG

School of Electronics and Information Engineering, Harbin Institute of Technology (Shenzhen), Shenzhen 518055, *China*

Received 8 May 2020/Revised 12 August 2020/Accepted 8 January 2021/Published online 24 December 2021

Abstract Reliable and efficient image transmission is crucial for deep-space exploration. However, the extremely long distance and complex deep-space environment introduce severe design and implementation challenges. In this work, we propose a novel high-efficiency system, CS-LTP-Spinal, to address the challenges encountered in deep-space image transmission. CS-LTP-Spinal is designed to work over the Licklider transmission protocol (LTP) of the delay-tolerant network (DTN). By incorporating compressed sensing (CS) and the Spinal codes as the application and physical layer techniques, CS-LTP-Spinal can satisfy the constraints originating from resource asymmetry between the space vehicles and the ground station. To match the time-varying deep-space channels, two coarse-grained rate-adaptive transmission strategies are designed that employ different CS decompression mechanisms based on erasure-tolerant and error-tolerant decompression, respectively, to exploit the robustness of CS reconstruction to erasures and errors. Then, the rates of CS compression and Spinal coding are optimized over the application, transport, and physical layers. A semi-physical deep-space communication platform is built, and extensive simulations on the Mars-to-Earth scenario are conducted. The results demonstrate that the designed CS-LTP-Spinal system with cross-layer optimized rate-adaptive transmission strategies has significant performance advantages over its counterparts by achieving near-ideal image transmission efficiency.

Keywords deep-space image transmission, CS-LTP-Spinal, rate-adaptive, cross-layer optimization, semi-physical simulation

Citation Wu S H, Li D Q, Jiao J, et al. CS-LTP-Spinal: a cross-layer optimized rate-adaptive image transmission system for deep-space exploration. Sci China Inf Sci, 2022, 65(1): 112303, https://doi.org/10.1007/s11432-020-3164-5

1 Introduction

Deep-space communication systems are responsible for data exchange between ground stations and remote space vehicles [1]. One of the core tasks of deep-space exploration is to successfully transmit various types of data such as images of a remote planet's surface, from space back to the ground station [2]. However, the extremely long distance and the complex electromagnetic environment have created significant challenges in the design of deep-space image transmission systems. The images to be transmitted are immense, which requires high efficiency in the transmission links. Moreover, the remote images are expected to provide the most intuitive information for analysis of unknown deep-space environments; therefore, reliable image transmission back to Earth is critically important. However, the design and implementation of high-efficiency image compression algorithms and high-gain channel coding techniques face several challenges.

• **High signal attenuation with significant time variance.** The deep-space channel suffers severely from high signal attenuation. In addition, several factors such as the rain and atmospheric loss, result in an extremely low and highly dynamic signal-to-noise-ratio (SNR) [3].

• **Long propagation delay and intermittent disruptions.** The propagation delay is extremely long and time varying. Even planet rotation can cause intermittent channels. This means that high-frequency feedback would be very inefficient for deep-space image transmission.

* Corresponding author (email: hitwush@hit.edu.cn)

• **Asymmetric resources.** The computation, storage, and energy resources of the remote space vehicles are limited, while those of the ground station are abundant [2]. Therefore, for image compression, the encoding complexity should be as low as possible, whereas the decoding complexity should be relatively high. For channel coding, both encoding and decoding complexity should be low because in cases of multi-hop transmission, the relay node needs to conduct both decoding and encoding.

To address these challenges, abundant research has been conducted on the design of deep-space image transmission systems. The delay-tolerant network (DTN) [4], which was designed for scenarios with long delay and frequent disruptions, has shown great potential in recent years to be the protocol stack for deep-space communication. For the transport layer of DTN, the newly-developed Licklider transmission protocol (LTP) [5] was designed specifically to operate over long-haul hops. A substantial amount of studies have also been conducted on image compression and channel coding algorithms individually to enhance the efficiency and reliability of deep-space image transmission [6,7]. However, the following issues remain and require further improvement.

In previous studies, image compression and channel coding are mainly implemented separately while neglecting the high implementation complexity. In addition, the dynamic nature of deep-space channels has not been fully explored thus far. The designed transmission strategies are mainly fixed rate, including the Chang'e-3 Lunar Rover [8] and the Jet Propulsion Laboratories (JPL) for the Mars Exploration Rover (MER) mission [9], which has led to underutilization of deep-space channels. In fact, rate-adaptive strategies based on appropriate use of feedbacks can obtain much higher transmission efficiency. Although for deep-space channels, high-frequency feedbacks should not be expected, low-frequency feedbacks that can indicate large time-scale channel dynamics such as the rain loss can be reasonably used. Further, joint allocation of the rates of image compression and channel coding can achieve optimal transmission performance under certain channel conditions [6].

To address the aforementioned issues, we propose a novel deep-space image transmission system designed to work over LTP incorporated with compression and coding algorithms that satisfy the constraints of asymmetrical resources. In addition, rate-adaptive strategies with cross-layer optimization are proposed to improve the transmission efficiency. For source compression, we adopt compressed sensing (CS) [10], which is known for its scalable compression and low encoding complexity, to realize compression with high efficiency yet low complexity. For channel coding, we adopt the Spinal codes [11], which can achieve near-capacity performance with a message length as short as 32 bits to realize affordable computation. For rate control, two coarse-grained rate-adaptive strategies are proposed to match the time-varying channel. They employ different CS decompression mechanisms, CS-erasure-tolerant and CS-error-tolerant, which originate from the robustness of CS reconstruction to erasures and errors, respectively. Furthermore, the rates of compression and channel coding are jointly optimized by cross-layer optimization. The proposed deep-space image transmission system is known as CS-LTP-Spinal. To verify the effectiveness of this system, we build a semi-physical simulation platform and run extensive simulations on the Mars-to-Earth transmission scenario. The results show that CS-LTP-Spinal can achieve near-ideal transmission efficiency.

The main contributions of this work are summarized below.

• A novel high-efficiency image transmission system known as CS-LTP-Spinal is proposed for deep-space exploration. Two coarse-grained rate-adaptive transmission strategies are designed for this system to dynamically match the time-varying deep-space channels.

• Cross-layer optimization methods for joint source-channel rate allocation of the two rate-adaptive transmission strategies are further proposed, by which the transmission efficiency of CS-LTP-Spinal is optimally explored.

• A semi-physical deep-space communication simulation platform is for implementing and testing the CS-LTP-Spinal system.

The remainder of this paper is organized as follows. Section 2 reviews the state-of-the-art studies in this field. In Section 3, we present the framework of CS-LTP-Spinal, the core techniques of which are briefly described. In Section 4, detailed rate-adaptive strategies are described, and the cross-layer optimization methods are given in Section 5. In Section 6, a case study of CS-LTP-Spinal on the Mars-to-Earth scenario is presented. The semi-physical platform and results are given in Section 7, and the conclusion is given in Section 8.

2 Related work

In previous deep-space missions such as the MER mission [9], widely used compression algorithms include the Joint Photographic Experts Group (JPEG) [12], JPEG2000 [13], and ICER [9]. These algorithms are mainly transform domain-based non-linear algorithms, which puts severe pressure on deep-space vehicles. The law of CS [10], which creates a linear projection of the source signals, indicates that if an image is sparse, it can be reconstructed with high probability from a much lower number of measurements than that based on the Nyquist sampling theory. Intuitively, owing to limitations in the computation, storage, and energy resources of the remote vehicles, CS appears to be a promising solution for such challenges.

For channel coding, conventionally codes include Reed-Solomon codes [14], convolution codes [15], and others. In recent years, advanced codes such as low-density parity check and Turbo codes have been widely adopted in space exploration [16]. However, near-capacity performance is achieved when moderate-to-long code words and iterative decoding mechanisms are used, resulting in prohibitively high complexity. Spinal codes, a novel type of rateless codes proposed by Perry et al. [11,17], have simple encoding structure and can nearly achieve the capacities of both the additive white Gaussian noise (AWGN) channel and the binary symmetric channel (BSC) with a message length as short as 32 bits. Moreover, the code rate can be modified adaptively by adjusting the number of passes.

To fully explore the transmission ability of the time-varying deep-space channel, the transmission strategy design should not aim only at the worst channel case [18]. Instead, it is expected that the transmission rate can self-adapt to the channel. In [19], the authors studied the performance of two classes of adaptive transmission schemes in a cellular downlink. One class was based on rateless codes with a power constant, and the other used fixed-rate codes with power adaptation. Ref. [20] considered the transmission control problem in a wireless senor system with a single-pixel image camera, and they formulated a more practical stochastic optimization problem for rate control and power control. However, they did not consider the impacts of channel feedback and the specific channel coding scheme. In [21], the authors proposed a combined optimal bit-rate-allocation algorithm to improve the efficiency in space exploration missions. The rate of each image was optimized under the overall bit rate constraint to minimize the overall distortion of a batch of images. However, these strategies rely on high-frequency low-layer feedbacks, which makes it unsuitable for deep-space communication.

An additional method for improving the transmission efficiency is cross-layer design. Its application to wireless transmission has been studied thoroughly [22, 23] with results showing strong potential for efficiency improvement. In [24], the authors presented a cross-layer design for data transmission consisting of rate control, routing, scheduling, and power control. They focused on the joint optimization over physical, MAC, network, and transport layers. Although few studies have been conducted on deep-space communication, the effectiveness of joint source-channel coding (JSCC) for deep-space image transmission has been preliminarily verified. Ref. [25] proposed a JSCC rate-allocation framework combining rate allocation and unequal error protection (UEP) to improve the image transmission performance. They designed an algorithm to select the optimal source and channel coding rate pair from pre-configured code rate sets. In [18], the authors presented a still image coding scheme using JSCC that introduces redundancy before source coding with real Bose-Chaudhuri-Hocquenghem (BCH) codes. Compared with a tandem scheme for a given channel situation, the JSCC scheme shows increased robustness as the channel conditions worsen. Ref. [6] proposed a new coding scheme for image transmission over noisy channels. They introduced a source-channel encoder after quantization to avoid the use of an explicit entropy coding stage, which is typically used in classical schemes.

In this study, it is the first to consider all design criteria of deep-space exploration to propose a high-efficiency deep-space image transmission system. The proposed CS-LTP-Spinal system is designed to work over the LTP of DTN, with CS and Spinal codes that can satisfy the constraints of asymmetrical node resources incorporated in the application and physical layers. Moreover, we use low-frequency high-layer feedbacks to coarsely infer the channel states for the transmitter, and we achieve coarse-grained adaptive rate controls to better explore the transmission ability of the time-varying deep-space channel. In our previous work [26], the framework of CS-LTP-Spinal was preliminarily designed. Further solid work is performed in the current study by exploiting the robustness of CS decompression to both erasures and errors.

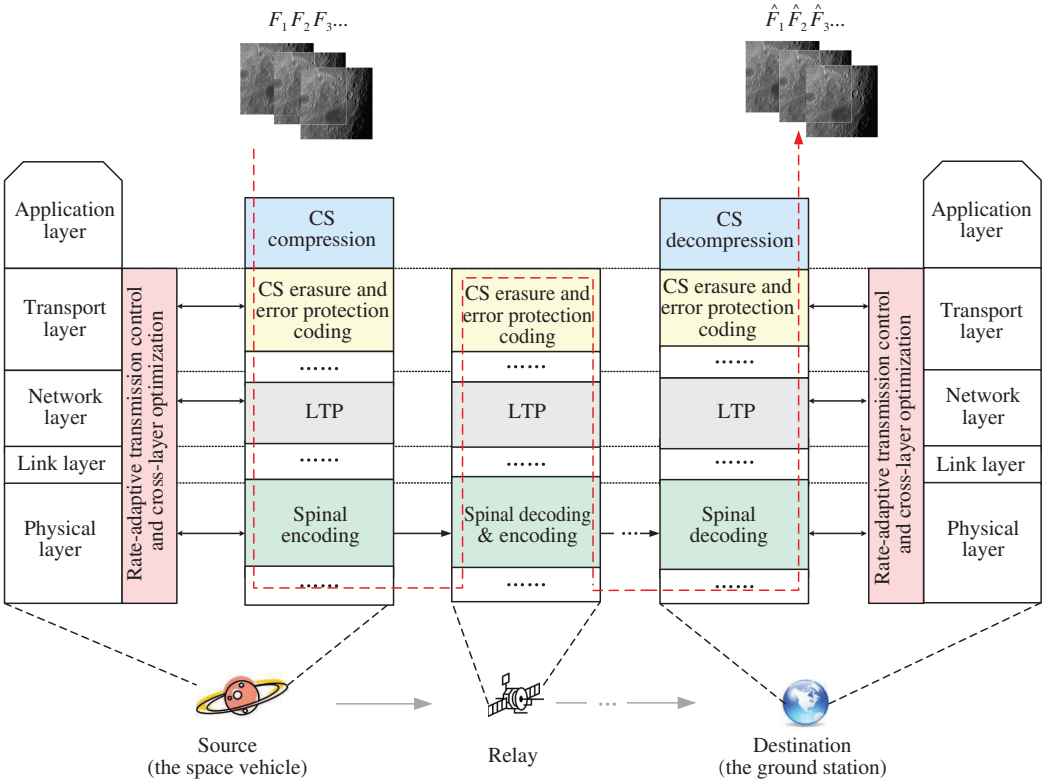

Figure 1 (Color online) Framework of the proposed CS-LTP-Spinal deep-space image transmission system.

3 Framework of the proposed CS-LTP-Spinal system

In this section, we present the framework of the proposed CS-LTP-Spinal system, and we briefly describe the basics of the three core technologies adopted.

3.1 CS-LTP-Spinal framework

As illustrated in Figure 1, three types of nodes—source, relay, and destination—are involved in the deep-space image transmission system. First, the remote space vehicle performs CS compression by a simple linear operation. Owing to the information-spreading nature of the linear operation, the CS decompression can achieve any required quality as long as sufficient amounts of compressed data are received. After the processing by the compression and erasure coding modules, the compressed data are submitted to the transport layer. Then, the output protocol data unit (PDU) stream is encoded in the physical layer by Spinal codes before being submitted to the relay. The relay decodes the Spinal blocks and checks whether the received data can meet the requirements of reconstruction. If so, the decoded packets will be re-encapsulated and sent to the ground. If not, the relay will send feedback to the source to request additional Spinal symbols. Finally, the ground station completes the decoding, decapsulation, and decompression. By rate-adaptive transmission control, the transmission rate is dynamically adjusted according to the low-frequency feedbacks from the receiver; by the cross-layer design, the CS, Spinal codes, and LTP are jointly optimized to obtain the optimal source-channel rate allocation.

3.2 CS image compression in the application layer

Let F denote the two-dimensional deep-space image to be compressed. $f \in \mathbb{R}^N$ denotes the vector form F. Suppose f is K-sparse in a certain domain Ψ; that is, the transform coefficients of f, denoted by α ($\alpha = \Psi f$), are mostly zero or close to zero. Φ is an $M \times N$ ($M \ll N$) matrix responsible for the compression operation, by which the CS compression results, denoted by $g \in \mathbb{R}^M$ are

$$g = \Phi f. \tag{1}$$

The decompression is formulated as the following constrained l_1 minimization problem provided that Θ satisfies the restricted isometry property (RIP) [27]:

$$\hat{\alpha} = \arg\min_{\alpha} \|\alpha\|_1 \quad \text{s.t.} \quad g = \Phi f = \Phi\Psi^{-1}\alpha = \Theta\alpha, \tag{2}$$

where $\|\cdot\|_1$ denotes the pseudo-norm, and $\Theta = \Phi\Psi^{-1}$ is the composite compression matrix. The decompressed image can be expressed as $\hat{f} = \Psi^{-1}\hat{\alpha}$. When Φ and Ψ are non-coherent, Θ satisfies RIP with high probability. Practically, the received compressed data is noise contaminated, which can be represented as $g = \Phi f + n$, where n is the noise. To decompress from the noisy compressed data, the l_1 minimization problem in (2) can be modified to

$$\hat{\alpha} = \arg\min_{\alpha} \|\alpha\|_1 \quad \text{s.t.} \quad \|g - \Theta\alpha\|_2 \leqslant \varepsilon, \tag{3}$$

where ε is set according to the noise level. In this study, Eq. (2) is a linear programming problem, and Eq. (3) is a second-order cone programming problem. Here, the block matching three-dimensional filtering denoiser-based approximate message passing (BM3D-AMP) is used as the reconstruction algorithm because it can provide state-of-the-art decompression performance, while operating tens of times faster than competitive methods [28, 29]. The most important property of CS decompression is its robustness to erasures and errors, which means that the decompression quality is guaranteed even if erasures occur. This property is based on the information-spreading operations of CS linear compression such that all of the compressed results are equally important, and more generated measurements result in better quality in the recovered image. The robust-to-error property is directly indicated by (3). To exploit the robustness of CS to erasures and errors, we propose CS-erasure- and CS-error-tolerant transmission strategies for rate-adaptive transmission control, the details of which are discussed in Section 4.

3.3 The LTP in the transport layer

After being processed by the CS compression and erasure coding, the compressed image data are processed by the lower layers of the DTN protocol stack. The bit stream is first divided into several bundles by BP protocol. Then, the bundles are aggregated, grouped, and transmitted to the transport layer, where LTP is used to add header and control information to realize reliable data transmission. When an LTP node contains data to send to its peer, it can open a session unilaterally and begin sending segments to the receiver. The transmitter is required to choose a unique session ID and to identify the receiver LTP application by its client service ID in all data segments. Retransmission-based reliability is offered in LTP by performing automated repeat request (ARQ) of lost data using the selective-acknowledgment model [5].

3.4 Spinal codes in the physical layer

The output of the upper layers will be encoded by Spinal codes in the physical layer, which is illustrated in Figure 2. First, the n-bit message A is grouped into n/k segments $\bar{a}_i$, $i \in 1, 2, \ldots, n/k$, each of which consists of k bits. Second, the encoder builds a spine of v-bit states by sequentially hashing together groups of k bits from A:

$$s_i = h(s_{i-1}, \bar{a}_i), \quad s_0 = 0^v, \tag{4}$$

where h is the Hash function, and s_0 is the initial spine vector. Finally, each random number generator (RNG) maps s_i into pseudo-random c-bit numbers that are converted into encoded symbols using a constellation mapping function. RNG is a deterministic function from a v-bit seed and an index to a c-bit number given by [17] as

$$\text{RNG}: \ \{0,1\}^v \times \mathbb{N} \to \{0,1\}^c, \tag{5}$$

and the encoder sends $\bar{x} = \left\{x_{1,j}, x_{2,j}, \ldots, x_{n/k,j}\right\}$ by j passes. As discussed in [17], the maximum likelihood decoding is the optimal decoder of Spinal codes, and the leaf node with the lowest decoding cost is considered as the decoding output. For the message A and its corresponding estimation $\hat{A}$, the decoding result is

$$\hat{A} = \arg\min_{A' \in (0,1)^n} \|\bar{y} - \bar{x}(A')\| = \arg\min_{A' \in (0,1)^n} \sum_{i=1}^{n/k} \sum_{j=1}^{L} \|\bar{y}_{i,j} - \bar{x}_{i,j}(\bar{a}')\|, \tag{6}$$

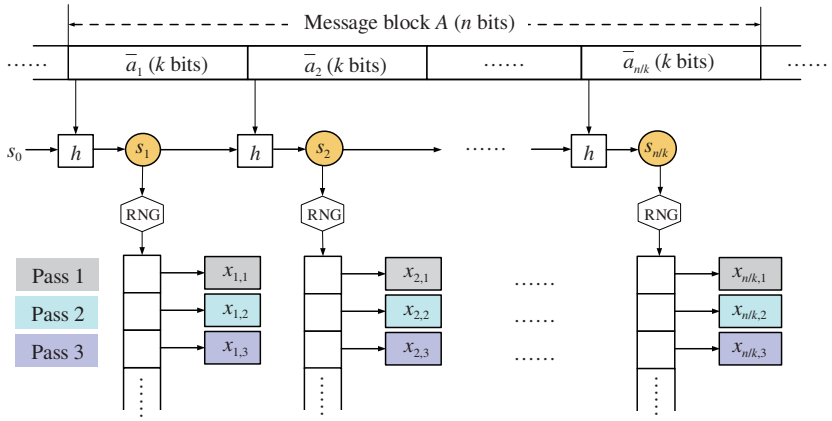

Figure 2 (Color online) Encoding process of Spinal codes.

where $\bar{y}$ denotes the received signal vector and the estimated message $\hat{A}$ is the one whose encoded vector $\bar{x}(\hat{A})$ is closest to $\bar{y}$. In this work, we use the sliding feedback decoding algorithm, which can reduce the decoding complexity while maintaining the performance of the Spinal codes. This model has been described in state-of-the-art work as a decoding algorithm of Spinal codes [30].

4 Rate-adaptive transmission strategy design

In this section, we characterize the time-varying deep-space channel and present the details of the two proposed rate-adaptive transmission strategies for CS-LTP-Spinal.

4.1 Time-varying deep-space channel

The deep-space channel is characterized by an extremely low and dynamically varying SNR, and the Ka-band is commonly used to satisfy the high bandwidth demand. Generally, the Ka-band deep-space channel can be modeled as an multi-state Markov chain, in which a time-slotted model is assumed [31]. The slot duration is set to be equal to the round trip time (RTT) of the transmission. Within each time slot, we assume that there are C possible channel states, with the tth state denoted by $G_t = j$ ($j \in \{1, 2, \ldots, C\}$). The state transition probability matrix is $\tilde{P}$, where p_{cj} ($c, j \in \{1, 2, \ldots, C\}$) denotes the transition probability from state c to state j when the transmission process changes from the current time slot to the next. For a certain value of C, the values of p_{cj} ($c, j \in \{1, 2, \ldots, C\}$) can be determined according to actual tracing results. For example, in [32], the authors divided the deep-space channel into good and bad states (i.e., $C = 2$). This model is referred to as the Gilbert-Elliott (GE) model.

We employed throughput to measure the transmission efficiency of the proposed system. To maximize the throughput, the transmitter should determine the number of Spinal symbols that should be transmitted for the current block before stopping to transmit for the next block. Aggressive transmission can cause decoding failure in the current block, resulting retransmission requests or a decrease in the final decompression quality, whereas conservative transmission can waste transmission resources.

In this study, cumulative distribution functions (CDF) of successful decoding of Spinal codes under different channel states are obtained with data generated from offline simulations. Let $\mathrm{CDF}(n_{\mathrm{Spinal}}|G_t = j)$ denote the successful Spinal decoding CDF under channel state j. The notation $\mathrm{CDF}(\cdot)$ is defined as $\mathrm{CDF}(x) = \Pr(X \leqslant x)$. When all of the blocks in a packet pass the cyclic redundancy check (CRC), the LTP packet is successfully received, and the probability is $\mathrm{CDF}(n_{\mathrm{Spinal}}|G_t = j)^{n_{\mathrm{CB}}}$, where n_{CB} is the number of blocks in each LTP packet. Hence, the packet loss rate can be expressed as $1 - \mathrm{CDF}(n_{\mathrm{Spinal}}|G_t = j)^{n_{\mathrm{CB}}}$.

In the coarse-grained rate-adaptive transmission strategy design, the CDF information is sent to the transmitter by the low frequency for transmission policy adjustment. Further details of the CDF modeling are presented in Section 6.

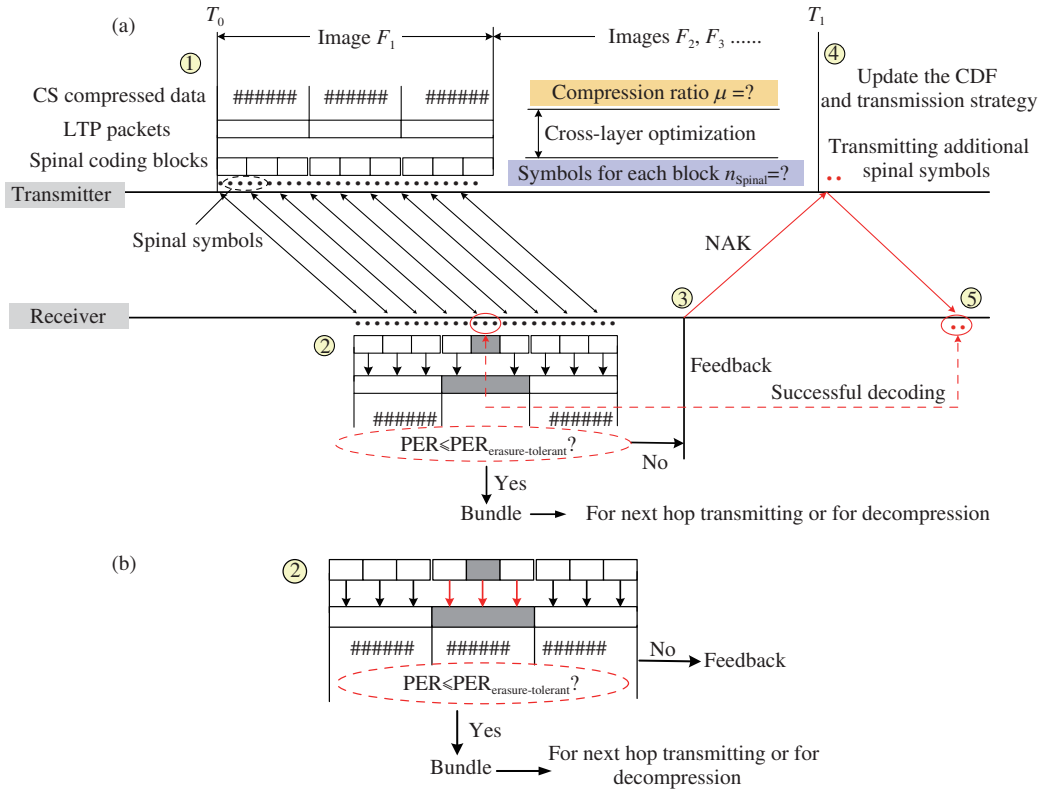

Figure 3 (Color online) (a) CS-erasure-tolerant-based rate-adaptive image transmission process and the corresponding cross-layer optimization; (b) step 2 of the CS-error-tolerant transmission process.

4.2 CS-erasure-tolerant-based rate-adaptive transmission strategy

In this subsection, we present the details of our proposed CS-erasure-tolerant transmission strategy, which exploits the CS decompression robustness to erasures. In this strategy, the receiver discards the erroneous LTP packets and keeps only the correct packets for upper layer processing. Figure 3(a) illustrates the details of the proposed strategy.

(1) At time T_0, the transmitter estimates the current channel state from the historical CDF and chooses an appropriate compression ratio μ for F_1. After CS compression, the compressed data are sent to lower layers. The compressed data are first divided into several bundles by BP protocol and are then encapsulated into several LTP packets to be forwarded to the next layer. When the packets reach the physical layer, they are divided into several coding blocks, each of which is attached with a CRC sequence and encoded by Spinal codes, with the number of symbols per coded spinal block as n_{Spinal}. After transmitting the image F_1, the following images $F_2, F_3, \ldots$ are successively sent instead of waiting for the acknowledgment (ACK).

(2) Upon receiving the spinal symbols, the receiver conducts decoding sequentially, conducting a CRC on each block and discarding the packets that have not passed the CRC. Simultaneously, the decoding CDFs are studied, and the indices of erroneous blocks are stored. After decoding and PDU unpacking, the receiver evaluates whether the packet error rate (PER) is within a certain range. If so, these data will be submitted to the bundle layer for next hop transmission or decompression.

(3) If the current PER cannot satisfy the decompression constraint, a negative acknowledgment (NAK) will be fed back to the transmitter by LTP, where the erroneous indices and the CDF are carried along.

(4) At T_1, if the source receives the NAK with the indices of erroneous blocks, it will send additional symbols. The CDF at the transmitter is then updated and will be used to adjust the following transmission strategy from "Aggressive" to "Conservative" by sending more spinal symbols or by decreasing the compression ratio. If the transmitter receives no NAK within one RTT (i.e., $T_1 - T_0$), the current channel condition is better than estimated, and the following transmission strategy can be adjusted from "Conservative" to "Aggressive".

(5) On receiving the additional symbols, the receiver uses both the additional and previously received

symbols to achieve successful decoding.

4.3 CS-error-tolerant-based rate-adaptive transmission strategy

The merits of CS-erasure-tolerant strategy are that data for decompression are all error-free, but this strategy has high requirements on the quality of channels. In the case of extremely dynamic deep-space channels, most of the packets would be discarded according to this strategy. And the application layer cannot obtain a sufficient number of compression values to guarantee the reconstruction quality.

To relieve the pressure on the decoding module and improve the efficiency, we further propose the CS-error-tolerant strategy by exploiting the robustness of the CS decompression to errors. This strategy enables the erroneous packets to reconstruct the image with the correct ones. In this process, steps 1 and 3–5 are the same as those used in the CS-erasure-tolerant strategy discussed in Subsection 4.2. The differences in step 2 are illustrated in Figure 3(b). In this step, the receiver conducts decoding sequentially and conducts a CRC on each decoded block. Then, it stores all of the data packets regardless of the erroneous state. The CRC results are then used to study successful CDF decoding online and to evaluate whether the PER satisfies the decompression constraint.

5 Problem formulation: cross-layer optimization

In this section, we present the cross-layer optimization problem formulation for the two rate-adaptive transmission strategies. The objective is to maximize the transmission throughput by adjusting the rates of CS compression and Spinal coding jointly with an image reconstruction quality constraint.

5.1 Cross-layer optimization for the CS-erasure-tolerant transmission strategy

As shown in the transmission process illustrated in Figure 3, the image F_1 is first compressed with a ratio μ:

$$\mu = (M \cdot Q)/(N \cdot P), \tag{7}$$

where N is the number of pixels in the image, M is the number of compression values, P is the quantization precision of each pixel, and Q is the quantization precision of each compression value.

Then, the output bit stream is encapsulated by the LTP protocol and the number of LTP packets is

$$N_{\mathrm{Pkt}} = \mu \cdot N \cdot P/(l_{\mathrm{Pkt}} - l_{\mathrm{Hdr}}), \tag{8}$$

where l_{Pkt} is the length of each LTP packet, and l_{Hdr} is the length of the packet header.

Then, each LTP packet is divided into n_{CB} Spinal blocks. n_{CB} can be calculated as

$$n_{\mathrm{CB}} = (l_{\mathrm{Pkt}} - l_{\mathrm{Hdr}})/l_{\mathrm{CB}}, \tag{9}$$

where l_{CB} is the size of each Spinal block. The number of Spinal blocks required to send F_1 is denoted by N_{CB} as

$$N_{\mathrm{CB}} = N_{\mathrm{Pkt}} \cdot n_{\mathrm{CB}}. \tag{10}$$

In Subsection 4.1, we defined the transition probability matrix by $\tilde{P}$, where p_{cj} $(c, j \in \{1, 2, \ldots, C\})$ denotes the probability of transiting from state c to j. We can determine the value of $G_{t-1} = c$ by the initial channel state information or the feedback CDF so that the transition probability vector from $t-1$ to the next moment is $p_t = [p_{c1}, p_{c2}, \ldots, p_{cC}]'$. Before the transmitter begins the next session, the PER of the LTP packets to be transmitted can be estimated as

$$\mathrm{PER} = 1 - [\mathrm{CDF}(n_{\mathrm{Spinal}}|G_t = 1)^{n_{\mathrm{CB}}}, \mathrm{CDF}(n_{\mathrm{Spinal}}|G_t = 2)^{n_{\mathrm{CB}}}, \ldots, \mathrm{CDF}(n_{\mathrm{Spinal}}|G_t = C)^{n_{\mathrm{CB}}}] \cdot p_t, \tag{11}$$

where n_{Spinal} is the number of symbols in each coded Spinal block, i.e., the parameter corresponding to the channel coding rate. After channel decoding, the receiver will discard the LTP packets that cannot pass the CRC, and the following reconstruction quality constraint should be applied:

$$\mathrm{PER} \leqslant \mathrm{PER}_{\text{erasure-tolerant}}(\mu), \tag{12}$$

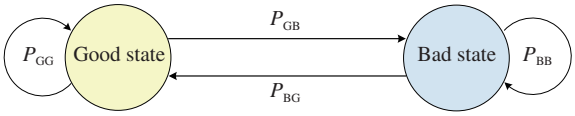

Figure 4 (Color online) Gilbert-Elliott model.

where μ is the current compression ratio, and $\mathrm{PER}_{\text{erasure-tolerant}}(\mu)$ is the corresponding maximum allowable PER for CS-erasure-tolerant-based image decompression. $\mathrm{PER}_{\text{erasure-tolerant}}(\mu)$ can be calculated as

$$\mathrm{PER}_{\text{erasure-tolerant}}(\mu) = (\mu - \mu_{\min})/\mu, \tag{13}$$

where $\mu_{\min}$ denotes the minimum compression ratio that can satisfy the required reconstruction quality when all of the compressed values are error-free.

The number of Spinal symbols required for transmitting each image is

$$N_{\text{Spinal}} = N_{\text{CB}} \cdot n_{\text{Spinal}}. \tag{14}$$

Our objective is to minimize N_{Spinal}, which is equivalent to maximizing the number of images transmitted per unit time, i.e., the throughput of the CS-LTP-Spinal system. By substituting the above equations into the optimization problem in (17), the optimal μ and n_{Spinal} can be expressed as

$$(\hat{\mu}, \hat{n}_{\text{Spinal}}) = \arg \min_{(\mu, n_{\text{Spinal}})} \{N_{\text{Spinal}}\} \quad \text{s.t.} \quad Eq.(12). \tag{15}$$

5.2 Cross-layer optimization for the CS-error-tolerant transmission strategy

Different from the strategy described in Subsection 4.2, the CS-error-tolerant strategy allows all of the decoded blocks, including the erroneous blocks, to be passed to the application layer for CS decompression. We take advantage of the robustness of CS-decompression-to-errors to further improve the transmission efficiency. The objective of the CS-error-tolerant strategy also maximizes the transmission throughput, which can be equivalently treated as minimizing N_{Spinal}. The related variables can still be calculated using (7)–(11), where the PER constraint is now given by

$$\mathrm{PER} \leqslant \mathrm{PER}_{\text{error-tolerant}}(\mu), \tag{16}$$

where $\mathrm{PER}_{\text{error-tolerant}}(\mu)$ is the maximum affordable PER corresponding to a compression ratio of μ. The relationship of $\mathrm{PER}_{\text{error-tolerant}}(\mu)$ with respect to μ can be obtained by Monte-Carlo simulation, which will be discussed further in Subsection 6.2. The Spinal symbols required to transmit each image are expressed by (14). The optimal values of μ and n_{Spinal} of the CS-error-tolerant strategy can be obtained by solving the following problem:

$$(\hat{\mu}, \hat{n}_{\text{Spinal}}) = \arg \min_{(\mu, n_{\text{Spinal}})} \{N_{\text{Spinal}}\} \quad \text{s.t} \quad \text{Eq. (16)}. \tag{17}$$

6 Case study: Mars-to-Earth transmission scenario

In this section, we present a case study of the CS-LTP-Spinal system applied to the Mars-to-Earth communication scenario.

6.1 Parameter settings

As previously mentioned, we used the GE model [32] to simulate the channel of the Mars-to-Earth scenario. The state transition process of the GE model is illustrated in Figure 4. When the channel is in the good state, the bit error rate (BER) is e_{Good}, and the probability of holding good is P_{GG}. When errors burst, the state transmits to the bad state with P_{GB}, and the BER is e_{Bad}. The probability of holding this state is P_{BB}, and the transition probability between the two states is P_{BG}.

In [31], the atmospheric noise temperatures were collected at the Deep-Space Network Madrid site for 5356 days. The authors determined 20 K to be a fair threshold for dividing the channel into good and

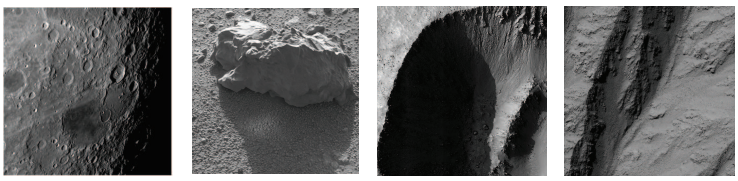

(a) (b) (c) (d)

Figure 5 Test images: (a) Moon surface, (b) Mars rock, (c) straight edge, (d) gullies of crater.

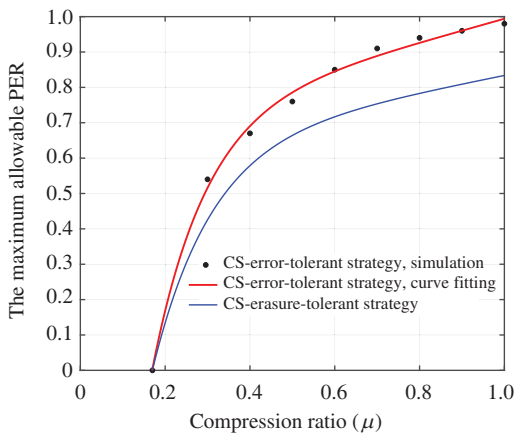

Figure 6 (Color online) Maximum allowable PER with respect to the compression ratio for the two transmission strategies.

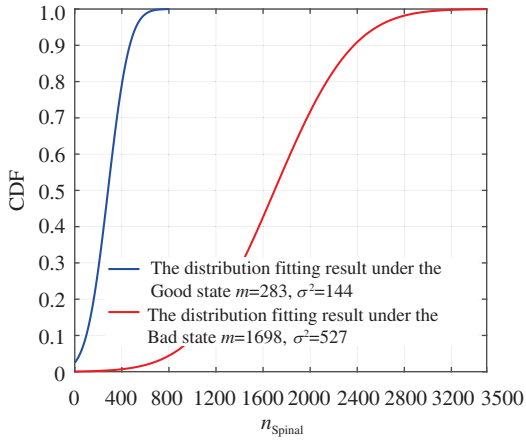

Figure 7 (Color online) Gaussian distribution fitting results for the successful decoding CDF under different channel states.

bad states, and they gave the following recommended BER values as follows: e_{Good} can be set as 10^{-8}, 10^{-7}, 10^{-6}, 10^{-5} and e_{Bad} can be set as 10^{-4} and 10^{-3}. The transition probability matrix is given by

$$\tilde{P} = \begin{bmatrix} P_{\text{GG}} & P_{\text{GB}} \\ P_{\text{BG}} & P_{\text{BB}} \end{bmatrix}, \tag{18}$$

where $P_{\text{GG}} = 0.9773$, $P_{\text{GB}} = 0.0227$, $P_{\text{BB}} = 0.8333$, $P_{\text{BG}} = 0.1667$.

Furthermore, we consider four test images sized 512×512, as shown in Figure 5 as "Moon surface", "Mars rock", "straight edge", and "gullies of crater". We adopted the BM3D-AMP decompression algorithm because it can provide state-of-the-art reconstruction performance while maintaining lower complexity, and Q was set to 5 bits. The minimum required CS decompression peak SNR (PSNR) was 30 dB. Moreover, for LTP protocol, l_{Pkt} was set to 1500 bytes, l_{Hdr} was set at 16 bytes, and l_{CB} was 32 bytes [3]. The parameters related to the Spinal codes were $n = 256$, $k = 4$.

6.2 Theoretical solutions to the cross-layer optimization problem

In addition to the parameter settings given in Subsection 6.1, two issues need to be specified to solve the two cross-layer optimization problems, i.e., (15) and (17).

• The maximum allowable PER that can satisfy the decompression requirements for a given compression ratio, i.e., the relationships of $\text{PER}_{\text{erasure-tolerant}}(\mu)$ in (12) and $\text{PER}_{\text{error-tolerant}}(\mu)$ in (16) with respect to μ. For the CS-erasure-tolerant strategy, the relationship of $\text{PER}_{\text{erasure-tolerant}}(\mu)$ with respect to μ is explicit, as shown by (13). For the CS-error-tolerant strategy, the relationship of $\text{PER}_{\text{error-tolerant}}(\mu)$ with respect to μ is not explicit and can be characterized by curve fitting in the Monte-Carlo simulation results. Figure 6 depicts the maximum allowable PER versus μ for the two transmission strategies.

• The successful decoding CDFs for Spinal decoding under different channel states, i.e., the $\text{CDF}(n_{\text{Spinal}}|G_t = j)$ in (11). Statistical results show that it can be well approximated with Gaussian distribution. A large number of Monte-Carlo simulations are performed for Spinal decoding under both good and bad states, with distribution fittings conducted over the decoding results. Figure 7 shows the Gaussian distribution fitting results, where the mean is denoted by m, and the variance is denoted by σ^2.

Table 1 Cross-layer optimization result

CS-erasure-tolerant strategy			CS-error-tolerant strategy		
Parameter	Good state	Bad state	Parameter	Good state	Bad state
$\hat{\mu}$	0.34	0.38	$\hat{\mu}$	0.61	0.68
$\hat{n}_{\text{Spinal}}$	768	1536	$\hat{n}_{\text{Spinal}}$	352	768

According to the parameter settings and the results in Figures 6 and 7, the two optimization problems shown in (15) and (17) can be solved. The solutions are given in Table 1.

6.3 Theoretical average throughput

According to (18), the stationary distribution probability of the good and bad states is

$$\begin{cases} P_{\text{GOOD}} \times 0.9773 + P_{\text{BAD}} \times 0.1667 = P_{\text{GOOD}}, \\ P_{\text{GOOD}} + P_{\text{BAD}} = 1, \end{cases} \tag{19}$$

where the solutions are $P_{\text{GOOD}} = 1667/1894$ and $P_{\text{BAD}} = 227/1894$. Thus, the theoretical average throughput of the proposed system can be expressed as

$$V = P_{\text{GOOD}} \cdot V_{\text{GOOD}} + P_{\text{BAD}} \cdot V_{\text{BAD}}. \tag{20}$$

Taking the CS-erasure-tolerant case as an example, the RTT is set to 30 min, and the bandwidth is set to 1 Mbps. Based on general formulation, we can calculate the number of images that can be transmitted in one RTT as $N_{\text{G}} = 840$ and $N_{\text{B}} = 375$, respectively. When the current channel state is good, the compression ratio μ is 0.34, and the number of Spinal symbols in one coded block $n_{\text{Spinal\_G}}$ is 768. When the channel state is good, the probability of successful decoding $P_{\text{GOOD\_GOOD}}$ is 0.845, and the value is larger than $1-\text{PER}_{\text{erasure-tolerant}}(\mu)$. Therefore, there is no need for feedback. However, when the channel state changes from the good to the bad state, the probability of successful decoding $P_{\text{GOOD\_BAD}}$ is 0.002, which is less than $1-\text{PER}_{\text{erasure-tolerant}}(\mu)$; therefore, it is necessary to request additional symbols in this case. According to the solutions of the cross-layer optimization for the bad state, we set the number of additional Spinal symbols $n_{\text{add\_G}}$ to 768, and the average time to process the feedback is

$$t_{\text{fb\_G}} = P_{\text{GB}} \cdot (1 - P_{\text{GOOD\_BAD}}) \cdot n_{\text{add\_G}}/n_{\text{Spinal\_G}} \cdot \text{RTT}. \tag{21}$$

The theoretical average throughput for the good state can be calculated by

$$V_{\text{GOOD}} = F_{\text{size}} \cdot N_{\text{G}}/(t_{\text{fb\_G}} + \text{RTT}). \tag{22}$$

When the current channel state is bad, μ is 0.38, $n_{\text{Spinal\_B}}$ is 1536. When the channel changes from the bad to good state, the probability of successful decoding $P_{\text{BAD\_GOOD}}$ is 1, which is larger than $1-\text{PER}_{\text{erasure-tolerant}}(\mu)$. Therefore, there is no need for feedback. However, when the channel changes from the good to bad state, the probability of successful decoding $P_{\text{BAD\_BAD}}$ is 0.394, which is less than $1-\text{PER}_{\text{erasure-tolerant}}(\mu)$. Hence, it is necessary to request additional data, and the number of additional Spinal symbols $n_{\text{add\_B}}$ is 352. The average time to process the feedback is

$$t_{\text{fb\_B}} = P_{\text{BB}} \cdot (1 - P_{\text{BAD\_BAD}}) \cdot n_{\text{add\_B}}/n_{\text{Spinal\_B}} \cdot \text{RTT}. \tag{23}$$

Thus, the theoretical average throughput for the bad state can be calculated by

$$V_{\text{BAD}} = F_{\text{size}} \cdot N_{\text{B}}/(t_{\text{fb\_B}} + \text{RTT}). \tag{24}$$

With the above results and channel state transition probability matrix, the expected value of theoretical average throughput can be expressed as

$$V_{\text{erasure-tolerant}} = P_{\text{GOOD}} \cdot V_{\text{GOOD}} + P_{\text{BAD}} \cdot V_{\text{BAD}} = 0.848 \text{ Mbps}. \tag{25}$$

For the CS-error-tolerant strategy, we get $N_{\text{G}} = 867$ and $N_{\text{B}} = 420$, respectively. Other parameters can also be calculated by (21)–(24), with the optimization results shown in Table 1. The theoretical average throughput can be expressed by

$$V_{\text{error-tolerant}} = P_{\text{GOOD}} \cdot V_{\text{GOOD}} + P_{\text{BAD}} \cdot V_{\text{BAD}} = 0.884 \text{ Mbps}. \tag{26}$$

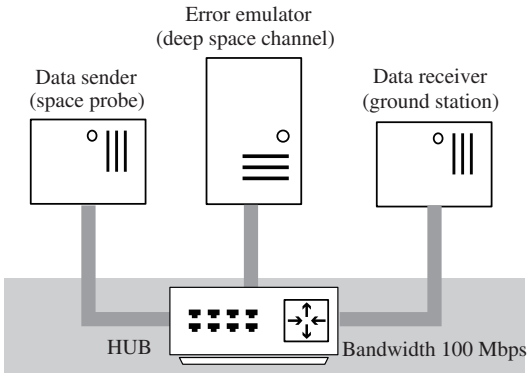

Figure 8 Setup of the semi-physical simulation platform.

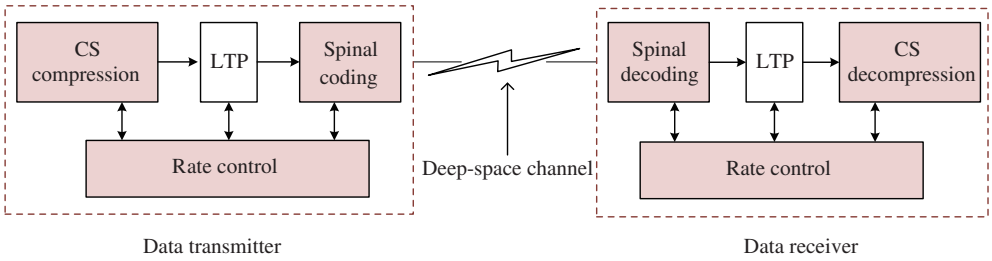

Figure 9 (Color online) Module diagram of the semi-physical platform.

7 Simulation setup and results

In this section, we first introduce the semi-physical simulation platform for CS-LTP-Spinal. Then, the performance of the proposed CS-LTP-Spinal system and its several counterparts are tested and compared.

7.1 Semi-physical simulation platform setup

To verify and evaluate the performance of the proposed CS-LTP-Spinal system, we established a semi-physical platform for the Mars-to-Earth scenario. Figure 8 shows a block diagram of the semi-physical platform. Our tests required three machines: the data sender, the data receiver, and the error emulator. The data sender machine models the space vehicle such as a spacecraft sending image data on the downlink; the data receiver models the ground station such as an antenna site receiving the data beamed to it; and the error emulator machine models the deep-space channel by emulating a configured error rate on the channel. Bandwidth and delay are emulated directly on the end-nodes. We studied the one-hop scenario and used three computers with the Linux system to set up the platform. They were connected by a HUB transponder, and the images were exchanged through a local area network with a bandwidth of 100 Mbps.

As illustrated in Figure 9, we design four modules at the node of the transmitter and receiver under DTN, including the CS module, LTP module, Spinal coding module, and rate control module. In the module of image compression/decompression, we use the Bernoulli matrix as the compression matrix and the BM3D-AMP algorithm as the CS image reconstruction algorithm. The purpose of LTP module is to realize reliable transmission control. After the encapsulation of LTP, the bit stream is encoded by Spinal codes in the channel coding module, and the Spinal symbols are then passed to the error emulation node through the socket communication. The function of the rate control module is to dynamically match the transmission rate to the time-varying deep-space channels. Although the errors are emulated in the middle node, delay and bandwidth are emulated in the end-nodes themselves via the Linux traffic control module. At the error emulation node, we emulate 1 Mbps end-to-end bandwidth and set the RTT to 30 min. Random errors are introduced to the received data by the error generation program according to the parameter settings given in Subsection 6.1.

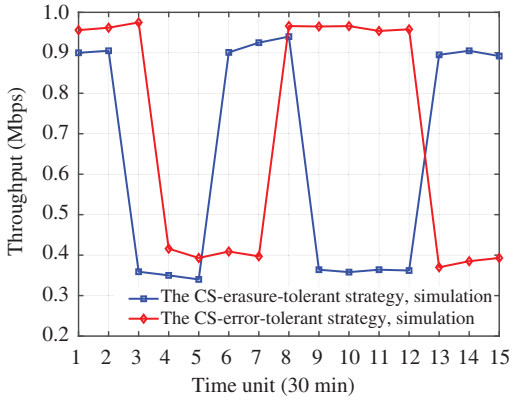

Figure 10 (Color online) Performance of the two proposed transmission strategies ($w = 1$ RTT).

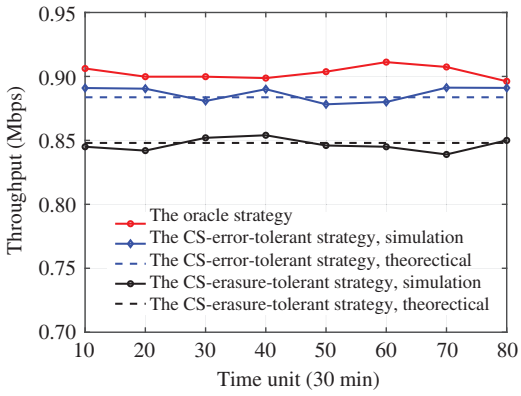

Figure 11 (Color online) Performance comparison of the two proposed transmission strategies ($w = 10$ RTTs).

7.2 Results and discussion

In this subsection, we present the performance of CS-LTP-Spinal and compare it with some related transmission strategies.

7.2.1 *Performance analysis of the proposed CS-LTP-Spinal system and transmission strategies*

First, the performance of the proposed CS-LTP-Spinal with two rate-adaptive transmission strategies is simulated and compared with four other conventional transmission strategies as follows.

(1) The oracle transmission strategy. Oracle indicates that the transmitter knows the channel state. Thus, it can precisely choose the appropriate parameters, and the receiver can successfully decode the Spinal blocks.

(2) The proposed CS-erasure-tolerant strategy. This strategy discards the packets that cannot pass the CRC. Upon receiving the NAK from the receiver, the transmitter additionally sends a certain number of Spinal symbols to the receiver and adjusts the subsequent strategy by historical CDF and channel state prediction.

(3) The proposed CS-error-tolerant strategy. This strategy allows all the packets, including the erroneous ones, to be used for image decompression; the other steps are the same as those in (2).

(4) The retransmission strategy with channel state prediction, abbreviated as RT-with-CP strategy. In this strategy, the transmitter can select the appropriate μ and n_{Spinal} for the next moment based on the historical CDF and repeats the current data upon receiving NAK instead of sending additional Spinal symbols.

(5) The retransmission strategy without channel state prediction, abbreviated as RT-without-CP strategy. This strategy is commonly used and is different from (2) and (3) in two aspects. The erroneous blocks will be retransmitted when receiving the NAK, and the transmitter cannot predict the channel state.

(6) The additional-transmission strategy without channel state prediction, abbreviated as AT-without-CP strategy. This strategy has no channel prediction mechanism, and the transmitter will send additional Spinal symbols when receiving the NAK feedback instead of retransmitting.

Figure 10 shows the performance results of the two proposed strategies when the window width (w) is set to 1 RTT. The channel state is always varying, and the transition of channel state causes changes in throughput. Figure 11 shows the performance when $w = 10$ RTTs. The simulation curves perfectly match the theoretical curves, whereas the observation time is relatively long, and it validates the correctness of the semi-physical platform. Figure 11 also shows that the throughput of the proposed strategies is very close to the oracle strategy. This shows that we can realize near-ideal transmission through the rate-adaptive design and cross-layer optimization. Therefore, the results validate the effectiveness of the proposed strategies.

Table 2 shows the PSNR of the test images in the case of employing the two proposed rate-adaptive transmission strategies using the optimal parameters given in Table 1. The achieved reconstruction performance is always greater than 30 dB regardless of whether the state is good or bad. Moreover,

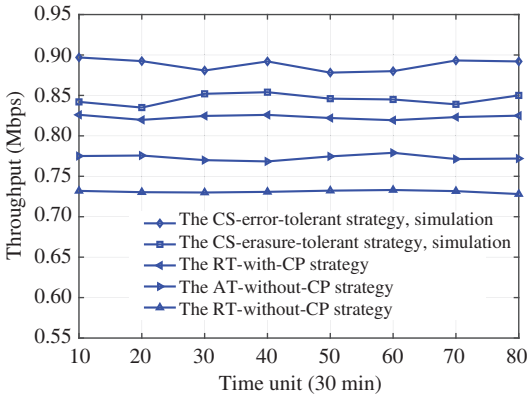

Figure 12 (Color online) Performance comparison of five different transmission strategies ($w = 10$ RTTs).

Table 2 Reconstructed results of test image based on the proposed transmission strategies

Transmission strategy	PSNR metric (dB)							
	Moon surface		Mars rock		Straight edge		Complex gullies	
	Good	Bad	Good	Bad	Good	Bad	Good	Bad
CS-erasure-tolerant	33.5	32.2	31.5	32.1	33.3	32.9	31.6	32.2
CS-error-tolerant	36.1	35.5	31.9	32.7	34.1	32.8	31.5	32.2

Figure 12 shows a throughput comparison of our proposed strategies and other existing strategies on the simulation platform. The two proposed rate-adaptive transmission strategies with low-frequency feedbacks have an advantage over the other transmission strategies. When compared with RT-without-CP strategy used by JPL for the MER mission, the throughput increases 16% and 20.5% by CS-erasure-tolerant and CS-error-tolerant strategies, respectively. This implies that the proposed rate-adaptive transmission strategies and cross-layer design can obtain a significant gain in transmission efficiency with respect to the conventional strategies.

7.2.2 *Comparison of CS-LTP-Spinal and state-of-the-art system*

We then compare the proposed CS-LTP-Spinal system with a related state-of-the-art deep-space image transmission system introduced in [25]. For the purpose of this comparison, we briefly present the baseline system in [25]. The baseline system is based on a joint source-channel rate-allocation approach in which a rate-allocation algorithm based on sliding comparison of PER is incorporated with a UEP scheme. The system adopts the SPIHT compression and Polar codes to implement the source and channel coding module, respectively, owing to their superiority over the counterparts. In the proposed rate-allocation algorithm, the optimal source and channel coding rate pair are selected from pre-configured code rate sets by sliding search. Furthermore, different channel coding rates are applied on sub-packets of source coding output packets to achieve UEP.

• **Comparison of system efficiency for a fixed target PSNR.** First, we consider a scenario in which the target PSNR is fixed. For a given set of test images in Figure 5, we compare the two systems in terms of system transmission rate R_{T} versus the channel state reflected by E_b/N_0 for the same target PSNR. The relationship of the system transmission rate R_{T}, source compression ratio, and channel coding rate is $R_{\mathrm{T}} = R_{\mathrm{s}}/R_{\mathrm{c}}$, and the system efficiency is reflected by R_{T}. The simulations are conducted over the AWGN channel with E_b/N_0 ranging from 1 dB to 4 dB, which is a typical SNR range for space communication scenarios [33]. For the example considered in this study, the target PSNR is 30 dB for all strategies, and the pre-configured source and channel code rate sets of the baseline system are given as follows:

$$\mathbb{R}_s = \{0.1, 0.25, 0.3, 0.35, 0.4, 0.5, 2/3, 8/11, 8/10, 8/9, 1.0\},$$

$$\mathbb{R}_c = \{1/50, 1/10, 1/8, 2/11, 1/4, 1/3, 4/11, 4/10, 4/9, 4/7, 3/5, 3/4, 4/5, 9/10\}.$$

For a given channel state, the baseline system chooses the optimal source and channel coding rate pair subject to the condition that the reconstruction PSNR must be higher than 30 dB. Figure 13(a) compares the resulting R_{T} vs. E_b/N_0 performance of the proposed two rate-adaptive transmission strategies in CS-LTP-Spinal with the JSCC strategy in the baseline system. The system transmission rates corresponding

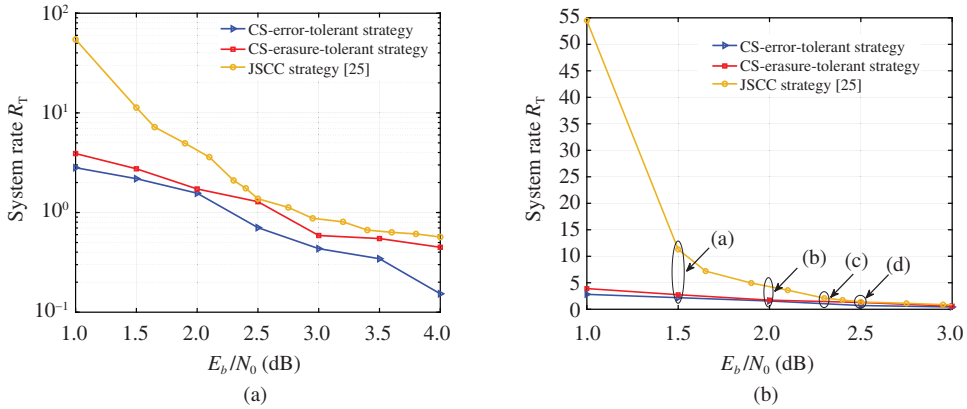

Figure 13 (Color online) (a) Rate performance of CS-LTP-Spinal and JSCC in [25]; (b) focus on E_b/N_0=2.5 dB point.

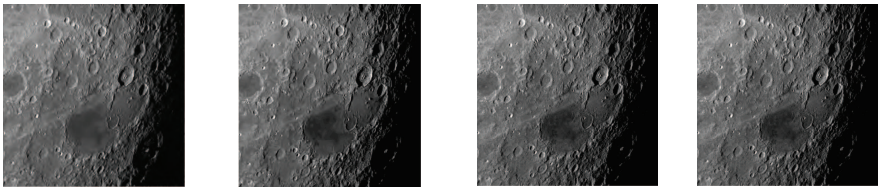

Figure 14 Reconstructed results of the Moon surface based on CS-error-tolerant strategy. (a) E_b/N_0=1.5 dB, PSNR=27.8 dB; (b) E_b/N_0=2 dB, PSNR=28.2 dB; (c) E_b/N_0=2.3 dB, PSNR=29.1 dB; (d) E_b/N_0=2.5 dB, PSNR=30 dB.

to the optimal solutions decrease with an increase in E_b/N_0 for all transmission strategies. That is, for a target PSNR, the proportion of redundancy required by channel protection decreases with an increase in E_b/N_0. Further, the CS-error-tolerant strategy performs slightly better than the CS-erasure-tolerant strategy in R_T. These results confirm the theoretical analysis given in Subsections 6.2 and 6.3. Further, Figure 13(a) shows that our proposed strategies can provide a superior rate performance over that of the baseline system, particularly in the low E_b/N_0 region. This is attributed to the use of advanced CS compression and Spinal coding, which can effectively meet the requirements of deep-space image transmission, and the two proposed coarse-grained rate-adaptive strategies, which can flexibly adjust the code rate to match the time-varying deep-space channel.

• **Robustness against mismatch between actual and the nominal channel conditions.** We then consider a situation in which the actual channel state does not match the nominal channel state. For example, we focus on a particular channel $E_b/N_0 = 2.5$ dB. We provide a zoomed version of Figure 13(a) around this value in Figure 13(b). We assume that the transmitter selects the optimal source-channel code rate pair (baseline system and proposed CS-LTP-Spinal) for the nominal $E_b/N_0 = 2.5$ dB, where the actual value is lower than 2.5 dB. In this case, the system transmission rate of the baseline system shows a significant decrease (indicated by the slope), whereas R_T of our proposed CS-LTP-Spinal system based on rate-adaptive transmission strategies gradually degrades. This indicates that the baseline system is highly sensitive to the change in channel state, with even a small change causing a significant loss of system efficiency. This is because the optimal code rate pair of the baseline system is selected from the discrete pre-configured code rate sets, which cannot change according to the dynamic deep-space channel. However, in our proposed CS-LTP-Spinal system, the rate-adaptive transmission strategies can dynamically adjust the source and channel code rate to match the time-varying deep-space channel. Therefore, the CS-LTP-Spinal system quipped with two transmission strategies has better built-in robustness to handle mismatched channel conditions. Furthermore, the PSNR in visual perception of the Moon surface image around 2.5 dB, based on the CS-error-tolerant transmission strategy, is shown in Figure 14, in which (a)–(d) indicate various mismatched E_b/N_0 values. The perceptive quality of the reconstructed image gradually degrades, and the perceived image quality is deemed acceptable over a wide range of channels E_b/N_0 even if the channel E_b/N_0 is as far as 1 dB lower than its nominal value of 2.5 dB.

8 Conclusion

In this study, we clarify a method for improving the transmission efficiency in a deep-space image transmission system through rate-adaptive transmission and cross-layer design. We first propose a novel high-efficiency image transmission system, CS-LTP-Spinal, for the deep-space scenario. In the CS-LTP-Spinal system, the CS and the Spinal codes jointly work with LTP under the DTN. On the basis of the proposed system, we design two coarse-grained rate-adaptive strategies to fit the dynamic channels, and we adopt a cross-layer design for joint source-channel rate allocation. Moreover, a semi-physical deep-space communication simulation platform is built to implement and test the system. Extensive simulations are conducted for performance evaluation. The results reveal that the CS-LTP-Spinal system can achieve near-ideal performance and significantly outperforms counterpart strategies.

Acknowledgements This work was supported in part by National Natural Science Foundation of China (Grant Nos. 61871147, 61831008, 62071141, 61525103, 61371102) and Guangdong Special Support Plan (Grant No. 2016TX03X226).

References

1 Zhao K L, Zhang Q Y. Network protocol architectures for future deep-space internetworking. Sci China Inf Sci, 2018, 61: 040303
2 Burleigh S, Cerf V G, Crowcroft J, et al. Space for Internet and Internet for space. Ad Hoc Networks, 2014, 23: 80–86
3 Xu G, Song Z. Effects of solar scintillation on deep space communications: challenges and prediction techniques. IEEE Wireless Commun, 2019, 26: 10–16
4 Wan P, Chen S, Yu T, et al. A hybrid multiple copy routing algorithm in space delay-tolerant networks. Sci China Inf Sci, 2017, 60: 042301
5 Yang G, Wang R, Burleigh S C, et al. Analysis of Licklider transmission protocol for reliable file delivery in space vehicle communications with random link interruptions. IEEE Trans Veh Technol, 2019, 68: 3919–3932
6 Bursalioglu O Y, Caire G, Divsalar D. Joint source-channel coding for deep-space image transmission using rateless codes. IEEE Trans Commun, 2013, 61: 3448–3461
7 Xu H Z, Chen C, Zhu M, et al. Nonbinary LDPC cycle codes: efficient search, design, and code optimization. Sci China Inf Sci, 2018, 61: 089303
8 Dai S W, Wu J, Sun H X, et al. Chang'E-3 lunar rover's scientific payloads. Chin J Space Sci, 2014, 34: 332–340
9 Kiely A, Klimesh M. The ICER progressive wavelet image compressor. IPN Progress Report, 2003, 42: 155
10 Donoho D L. Compressed sensing. IEEE Trans Inform Theor, 2006, 52: 1289–1306
11 Perry J, Iannucci P A, Fleming K E, et al. Spinal codes. ACM SIGCOMM Comput Commun Rev, 2012, 42: 49–60
12 Amerini I, Uricchio T, Ballan L, et al. Localization of JPEG double compression through multi-domain convolutional neural Networks. In: Proceedings of IEEE CVPR Workshop on Media Forensics, Honolulu, 2017. 1865–1871
13 Liu F, Ahanonu E, Marcellin M W, et al. Visibility thresholds in reversible JPEG2000 compression. In: Proceedings of Data Compression Conference (DCC), Snowbird, 2017. 450
14 Shi L, Jiao J, Sabbagh A, et al. Integration of reed-solomon codes to Licklider transmission protocol (LTP) for space DTN. IEEE Aerosp Electron Syst Mag, 2017, 32: 48–55
15 Viterbi A. Convolutional codes and their performance in communication systems. IEEE Trans Comm Technol, 1971, 19: 751–772
16 Andrews K S, Divsalar D, Dolinar S, et al. The development of turbo and LDPC codes for deep-space applications. Proc IEEE, 2007, 95: 2142–2156
17 Perry J, Balakrishnan H, Shah D, et al. Rateless Spinal codes. In: Proceedings of the 10th ACM Workshop on Hot Topics in Networks, 2011. 1–6
18 Gabay A, Kieffer M, Duhamel P. Joint source-channel coding using real BCH codes for robust image transmission. IEEE Trans Image Process, 2007, 16: 1568–1583
19 Rajanna A, Dettmann C P. Adaptive transmission in cellular networks: fixed-rate codes with power control versus physical layer rateless codes. IEEE Trans Wireless Commun, 2019, 18: 3005–3018
20 Xiang S, Cai L. Transmission control for compressive sensing video over wireless channel. IEEE Trans Wireless Commun, 2013, 12: 1429–1437
21 Xu Y, Li J, Lin X, et al. An optimal bit-rate allocation algorithm to improve transmission efficiency of images in deep space exploration. China Commun, 2020, 17: 94–100
22 Peron G, Brante G, Souza R D, et al. Physical and MAC cross-layer analysis of energy-efficient cooperative MIMO networks. IEEE Trans Commun, 2018, 66: 1940–1954
23 Zhao X, Chen W. Non-orthogonal multiple access for delay-sensitive communications: a cross-layer approach. IEEE Trans Commun, 2019, 67: 5053–5068
24 Li C, Wang J, Li M. Data transmission optimization algorithm for network utility maximization in wireless sensor networks. Int J Distrib Sens Netw, 2016, 12: 155014771667064
25 Dong D, Wu S, Li D, et al. Joint source-channel rate allocation with unequal error protection for space image transmission. Int J Distrib Sens Netw, 2017, 13: 155014771772114
26 Luo J, Wu S, Xu S, et al. A cross-layer image transmission scheme for deep space exploration. In: Proceedings of IEEE Vehicular Technology Conference (VTC-Fall), Toronto, 2017. 1–5
27 Colonnese S, Rinauro S, Cusani R, et al. The restricted isometry property of the Radon-like CS matrix. In: Proceedings of IEEE International Workshop on Multimedia Signal Processing (MMSP), Pula, 2013. 248–253
28 Yang D, Sun J. BM3D-Net: a convolutional neural network for transform-domain collaborative filtering. IEEE Signal Process Lett, 2018, 25: 55–59
29 Metzler C A, Maleki A, Baraniuk R G. From denoising to compressed sensing. IEEE Trans Inform Theor, 2016, 62: 5117–5144
30 Xu S, Wu S, Luo J, et al. Low complexity decoding for spinal codes: sliding feedback decoding. In: Proceedings of IEEE Vehicular Technology Conference (VTC-Fall), Toronto, 2017. 1–5
31 Sung U I, Gao L J. CFDP performance over weather-dependent Ka-band channel. In: Proceedings of SpaceOps Conference, Rome, 2006. 1–5
32 Gilbert E N. Capacity of a burst-noise channel. Bell Syst Technical J, 1960, 39: 1253–1265
33 Huang K, Liang C, Ma X, et al. Unequal error protection by partial superposition transmission using low-density parity-check codes. IET Commun, 2014, 8: 2348–2355